PL-TR-91-2185

A WAVEFORM INVERSION TECHNIQUE FOR MEASURING ELASTIC WAVE ATTENUATION IN CYLINDRICAL BARS

Randolph J. Martin, III
Xiao Ming Tang

New England Research Inc
76 Olcott Drive
White River Junction, VT 05001

23 July 1991

Scientific Report No. 2

Approved for public release;
Distribution unlimited

PHILLIPS LABORATORY
AIR FORCE SYSTEMS COMMAND
HANSCOM AIR FORCE BASE, MASSACHUSETTS 01731-5000

SPONSORED BY
Defense Advanced Research Projects Agency
Nuclear Monitoring Research Office
ARPA ORDER NO. 5307

MONITORED BY
Phillips Laboratory
Contract FY19628-89-C-0097

This technical report has been reviewed and is approved for publication.

JAMES F. LEWKOWICZ
Contract Manager
Solid Earth Geophysics Branch
Earth Sciences Division

JAMES F. LEWKOWICZ
Branch Chief
Solid Earth Geophysics Branch
Earth Sciences Division

DONALD H. ECKHARDT, Director
Earth Sciences Division

REPORT DOCUMENTATION PAGE

Form Approved
OMB No 0704-0188

1. AGENCY USE ONLY *(Leave blank)*	2. REPORT DATE	3. REPORT TYPE AND DATES COVERED
	23 July 1991	Scientific Report No. 2

4. TITLE AND SUBTITLE
A Waveform Inversion Technique for Measuring Elastic Wave Attenuation in Cylindrical Bars

5. FUNDING NUMBERS
PE 62714E
PR 9A10 TA DA WUDB
Contract F19628-89-C-0097

6. AUTHOR(S)
Randolph J. Martin, III
Xiao Ming Tang

7. PERFORMING ORGANIZATION NAME(S) AND ADDRESS(ES)
New England Research Inc
76 Olcott Drive
White River Junction, VT 05001

8. PERFORMING ORGANIZATION REPORT NUMBER

9. SPONSORING/MONITORING AGENCY NAME(S) AND ADDRESS(ES)
Phillips Laboratory
Hanscom AFB, MA 01731-5000

Contract Manager: James Lewkowicz/LWH

10. SPONSORING/MONITORING AGENCY REPORT NUMBER
PL-TR-91-2185

11. SUPPLEMENTARY NOTES

12a. DISTRIBUTION/AVAILABILITY STATEMENT

Approved for public release;
Distribution unlimited

12b. DISTRIBUTION CODE

13. ABSTRACT *(Maximum 200 words)*

This report presents a new technique for measuring elastic wave attenuation in the frequency range of 10-150 kHz. The technique consists of measuring low-frequency waveforms using two cylindrical bars of the same material, but different lengths. The attenuation is obtained in two steps. First, the waveform, measured within the shorter bar, is theoretically propagated to the length of the longer bar. The distortion of the waveform due to the dispersion effect of the cylindrical waveguide is corrected for. Second, is the inversion for the attenuation, or Q of the rock, is obtained by minimizing the difference between the propagated waveform and the actual waveform measured within the longer bar. Because the waveform inversion is performed in the time domain, the waveforms can be appropriately truncated to avoid multiple reflections due to the finite size of the (shorter) sample, allowing attenuation to be measured at long wavelengths or low frequencies. The frequency range in which this technique operates fills the gap between the resonant bar measurement (~100-1000 kHz). Attenuation values in a PVC (a highly attenuative) material and in Sierra White granite were measured in the frequency range of 40-140 kHz. The attenuation for the two materials are found to be consistent with other measuring techniques.

14. SUBJECT TERMS
Attenuation
Rock Properties
Seismic Yield Estimation

15. NUMBER OF PAGES
32

16. PRICE CODE

17. SECURITY CLASSIFICATION OF REPORT	18. SECURITY CLASSIFICATION OF THIS PAGE	19. SECURITY CLASSIFICATION OF ABSTRACT	20. LIMITATION OF ABSTRACT
Unclassified	Unclassified	Unclassified	SAR

NSN 7540-01-280-5500

Standard Form 298 (Rev 2-89)
Prescribed by ANSI Std 239-18
298-102

CONTENTS

INTRODUCTION

Seismic wave attenuation in rocks is a very important parameter not only because it affects the seismic wave propagation through the earth, but also because it is a sensitive indicator of rock properties under various conditions. The main purpose of measuring attenuation in the laboratory is to use the data to infer rock properties at *in-situ* scales and seismic frequencies. Unfortunately, accurate measurements of intrinsic attenuation are difficult to obtain in both the laboratory and field, because other effects, like geometrical spreading, boundary reflections, also affect waveform amplitudes. In the laboratory, attenuation is usually measured using ultrasonic pulse propagation and resonant bar techniques. For the propagation of stress pulses through rock samples, attenuation can be estimated from the rise-time of the pulse on-set (Blair, 1982) or from using the spectral ratio technique (Toksöz et al., 1979). However, as pointed out by Liu (1988), the rise time is strongly affected by the source time function. The conversion from rise time to attenuation also assumes a specific attenuation model (e.g., constant-Q model, Kjartansson, 1979), which may become invalid in the presence of fluid saturation (Jones, 1986). The spectral ratio method derives attenuation from the slope of a line fitted to the logarithmic ratio of the spectra of two waveforms. Because waveforms may be affected by reflections from sample boundaries, high frequency pulses ($\sim$ 1 MHz) and samples with large lateral dimensions are used in the measurements (Toksöz et. al., 1979). Even so, signals may still have to be truncated to remove extra arrivals which may significantly affect the wave spectra. Moreover, the diffraction effects of the transducer source may need to be corrected for in such measurements (Tang et al., 1990). The resonant bar technique utilizes the resonance of a vibrating cylindrical rod. The resonant frequency of the fundamental mode usually occurs between 3$\sim$10 kHz, depending on the length of the rod. Because of the very different frequency ranges of the ultrasonic and resonant techniques, attenuations obtained from the two techniques can be significantly different (Blair, 1990). In addition, the resonant bar measurement is difficult to perform under pressure, whereas the pulse propagation method is most suited for use in pressure vessels. It is desirable to have a technique that measures attenuation in the low to medium frequency range in order to understand attenuation mechanisms in rocks as a function of wavelengths and of *in-situ* conditions. The purpose of this study is to develop a technique that combines the advantages of the two methods and operates in the low to medium frequency ranges.

A direct way of reducing the measurement frequency in the pulse propagation method is by using low frequency sources and increasing the propagation length between source and receiver transducers. However, because of the beam spreading of the transducer radiation, the lateral dimension of the sample must be increased proportionally to avoid the contamination of the direct signal by the reflections from lateral boundaries. This results in a large sample volume that is impractical for laboratory measurements. This problem can be avoided by using the cylinder-shaped sample as used in the resonant bar method. The use of the bar geometry in the pulse propagation method has two major advantages. First, the sample length can be chosen according the wavelength without having to increase lateral dimensions. Thus it is suited for use in pressure vessels and with saturated samples. Second, the fundamental mode in a cylindrical bar is a low frequency wave phenomenon whose propagation and dispersion characteristics are well understood and can be accurately modeled. Because the dispersion effects of the waveguide can distort the source signal into a long wave train (particularly at high frequencies), the spectral ratio technique is not suitable for this application. This method is most accurate with short duration signals. To overcome this, we have developed a waveform inversion technique that needs only the first few cycles of the waveforms to obtain reliable estimates of attenuation.

In the following studies, the propagation characteristics of the fundamental wave mode in a cylindrical bar will be discussed. Then the procedure for the waveform inversion technique will be formulated. Finally, the procedure is applied to measure attenuation in a PVC material and in Sierra White granite. The results for the granite are compared with those obtained using other techniques.

PROPAGATION OF THE FUNDAMENTAL WAVE MODE IN A CYLINDRICAL BAR

In a thin cylindrical rod consisting of an elastic material, propagation of extensional waves is governed by the Pochhammer equation (Kolsky, 1953)

$$(2l/a)(m^2 + k^2)J_1(la)J_1(ma) - (m^2 - k^2)^2 J_0(la)J_1(ma) - 4k^2 lm J_1(la)J_0(ma) = 0 \quad . \tag{1}$$

where a is bar radius, J_n $(n = 0, 1)$ is the nth order Bessel function, k is the extensional wavenumber, and

$$l = \sqrt{\omega^2/V_p^2 - k^2} \text{ and } m = \sqrt{\omega^2/V_s^2 - k^2}$$

are radial compressional and shear wavenumbers, V_p and V_s are compressional and shear velocities respectively, and ω is angular frequency. Although Eq. (1) gives rise to a number of extensional wave modes in the bar (Kolsky, 1953), the fundamental mode is of the most interest to us. At very low frequencies ($\omega \rightarrow 0$), the velocity of this mode approaches $V_e = \sqrt{E/\rho}$, where E is the Young's modulus and ρ is the density of the bar. With increasing frequency, the phase velocity of the mode decreases. Because of the change of velocity with frequency (i.e., velocity dispersion), the waveform of the mode will be distorted as the wave propagates along the bar. To demonstrate this effect, we consider the spectrum of the propagating wave at the distance x away from the source

$$W(\omega, x) = S(\omega)\exp(ikx) \quad , \tag{2}$$

where $S(\omega)$ is the spectrum of the transducer source. After solving Eq. (1), Eq. (2) can be transformed into time domain to obtain waveforms at various distances x. Figure 1a shows the phase velocity (dashed curve marked 'phase', obtained as ω/k) and group velocity (dashed curve marked 'group', obtained as $d\omega/dk$), as well as the amplitude of the source spectrum $S(\omega)$ (solid curve) as functions of frequency for this example. The results are calculated for a bar of 1 cm radius with $V_p = 4272$ m/s and $V_s = 2506$ m/s. The source is a Ricker source (Ricker, 1953) centered around 70 kHz. Figure 1b shows the synthetic waveforms at the distances x=0, 10, 20, and 30 cm from the source. Because the wave spectrum covers the frequency range where significant velocity dispersion occurs, the waveform is gradually distorted into a long wave train as it propagates along the bar. In addition, as indicated in Figure 1b, an Airy phase with very slow group velocity is developed, which is associated with the minimum on the group velocity curve (Figure 1a). For signals with such a long duration, the spectral method for attenuation estimation is not applicable. The complete wave spectrum may not be recovered by either truncating the signal or taking the complete wave train. The former approach removes a portion of the wave energy, while the latter, when measuring a sample of finite size, may include reflections that bounce back and forth between the source and receiver. One may also try to estimate attenuation by measuring the amplitude decay of the first arrival with distance. However, because of the dispersion effect, the wave amplitude decreases with distance even in the absence of intrinsic attenuation as in this example (Figure 1b). By studying this theoretical example, it is clear that any attempt to measure intrinsic attenuation using cylindrical bars will have to consider the change of waveform due to the dispersive nature of the waveguide. Fortunately, since this effect is well governed by Eq. (1), it can be accurately corrected for provided the parameters V_p, V_s, and a of the bar are given.

ESTIMATING ATTENUATION THROUGH WAVEFORM INVERSION

In the presence of intrinsic attenuation in the bar, the attenuation effect is taken into account by making the wavenumber k complex, as

$$k \longrightarrow k\left(1 + \frac{i}{2Q_e}\right) \quad . \tag{3}$$

where Q_e is the extensional quality factor of the bar material. As will be described later in the experimental procedure, the attenuation measurements are usually performed in a narrow frequency range. Therefore, even if Q_e can vary with frequency, it may be regarded as constant over the narrow frequency range. In addition, the anelastic wave dispersion is not included because the effect is negligible in this narrow frequency range.

The waveform inversion technique involves comparing the waveforms received using two bars of the same material but different lengths x_1 and x_2 ($> x_1$). In the two bars, the measurement conditions (i.e., the signal generation and receiver response) are assumed to be the same. From Eqs. (2) and (3), it is readily seen that the spectra of the two waveforms are related via

$$W(\omega, x_2) = W(\omega, x_1)\exp[ik(1 + i/2Q_e)(x_2 - x_1)] \quad . \tag{4}$$

or, transform into time domain

$$W(t, x_2) = W(t, x_1) * D(t) * A(t) \quad . \tag{5}$$

where

$$D(t) = F^{-1}\{\exp[ik(x_2 - x_1)]\} \text{ and } A(t) = F^{-1}\{\exp[-k(x_2 - x_1)/2Q_e]\}$$

are respectively designated as the dispersion operator and attenuation operator, the symbol $*$ denotes convolution, and $F^{-1}\{\cdots\}$ denotes taking the inverse Fourier transform. From Eqs. (4) and (5), it is clearly seen that the difference between the waveforms $W(t, x_2)$ and $W(t, x_1)$ is due to two effects. The first is the waveform distortion due to the velocity dispersion $[D(t)]$ along the $x_2 - x_1$ section of the cylindrical bar. The second is the amplitude decay due to the intrinsic damping $[A(t)]$ along the same section. The first effect can be corrected using the theory presented in the previous section. The second effect will be used to derive Q_e of the bar material. Although the waves in a cylindrical bar usually have long durations, the attenuation affects the first few cycles of the waveforms in much the same way as it affects the whole wave train. Based on this fact, the waveform inversion technique derives attenuation or Q_e from the first few cycles of the waveforms.

The waveform inversion procedure consists of two major steps. In the first, the measure waveform $W(t, x_1)$ is theoretically propagated to distance x_2, in which the effect of attenuation is not included. Mathematically, this operation is expressed as

$$\widetilde{W}(t, x_2) = W(t, x_1) * D(t) \quad , \tag{6}$$

where $\widetilde{W}(t, x_2)$ is the resulting waveform after the propagation. In this operation, if the velocities V_p and V_s are exact, $\widetilde{W}(t, x_2)$ will be aligned in phase with the measured waveform $W(t, x_2)$. In practice, a slight shift of $\widetilde{W}(t, x_2)$ may be necessary to obtain such an alignment, because the V_p and V_s used in calculating Eq. (6) are measured values and may contain errors. This first step may be called the dispersion correction. The second step is the inversion for attenuation or Q_e by minimizing the difference between $\widetilde{W}(t, x_2)$ and $W(t, x_2)$. To do so, we construct the following error function

$$\begin{aligned} E(Q_e) &= \int_{T_0}^{T_0+\Delta T} [W(t, x_2) - \widetilde{W}(t, x_2) * A(t)]^2 dt \\ &= \int_{T_0}^{T_0+\Delta T} \left[W(t, x_2) - F^{-1}\{\widetilde{W}(\omega, x_2) \exp[-k(x_2 - x_1)/2Q_e]\}\right]^2 dt \quad , \end{aligned} \tag{7}$$

where T_0 may be chosen as the beginning time of $W(t, x_2)$ and ΔT is the duration of the time section in which $\widetilde{W}(t, x_2)$ and $W(t, x_2)$ are matched. In the inversion using synthetic waveforms, ΔT can include any number of cycles of the waveforms without altering the inverted value of Q_e, because the waveform data are exact. For laboratory data, however, the measured waveforms always contain experimental errors (e.g., random electrical noise). Therefore, ΔT should be chosen as long as possible to reduce the effect due to the errors. In practice, ΔT may be chosen as $2x_1/V_e$, which, for the shorter sample, is approximately the arrival time difference between the direct arrival and the first reflection back from the source. The minimization is performed using the non-linear least squares procedure. We first assign a very rough estimate of Q_e. Then we multiply the spectrum $\widetilde{W}(\omega, x_2)$ with

$\exp[-k(x_2 - x_1)/2Q_e]$ and transform the product back to the time domain [because this operation mainly modifies the amplitude of $\widetilde{W}(t, x_2)$ without (significantly) altering its phase, the effects of multiple reflections will not be shifted into the interval ΔT]. If the estimated Q_e is not sufficient to make the resulting waveform match with $W(t, x_2)$, Q_e is perturbed following the method of non-linear least squares minimization (Moré, 1978) and the same procedure is repeated in an iterative manner until the error $E(Q_e)$ reaches a minimum. The value of Q_e at this minimum is taken as the estimated Q_e.

To summarize the procedure, we give an inversion example using synthetic waveforms. The waveforms are generated using the same parameters used in Figure 1. But now a Q_e of 50 is used in the calculation of the synthetic waveforms. The waveforms at $x_1 = 10$ cm and $x_2 = 30$ cm are used for the inversion. Figure 2a shows the waveforms. The waveform at 10 cm is theoretically propagated to 30 cm without including the attenuation (i.e., $Q_e = \infty$). Figure 2b shows that, after the propagation, waveform $\widetilde{W}(t, x_2)$ is aligned in phase with $W(t, x_2)$. However, the amplitudes of the two waveforms do not match because the attenuation effect was not included in the propagation. The next step is to minimize the amplitude difference between the two waveforms using the inversion technique. As shown in Figure 2b, only the first two cycles are used in the inversion. After the inversion, the two waveforms coincide with each other, as shown in Figure 2c. The Q_e value obtained from the inversion is 50.1, in close agreement with the true value of 50. It is noted that for synthetic data, the inverted Q_e is not sensitive to the number of cycles used in the inversion, because the data do not contain errors or effects of extra arrivals, such as multiple reflections.

The procedure of matching the first part of $\widetilde{W}(t, x_2)$ and $W(t, x_2)$ using the inversion technique has several major advantages. The first is that only the first few cycles of the waveforms are needed for the Q_e estimation. This separates the effect of intrinsic attenuation from the effect due to later arrivals (i.e., multiple reflections). The second advantage is that the solution to the inverse problem is unique because only one parameter Q_e is estimated. Finally and most importantly, the inversion is performed using the waveforms of the low frequency fundamental mode, allowing the attenuation to be measured in a much lower frequency range than that of the ultrasonic pulse propagation technique.

APPLICATION TO LABORATORY MEASUREMENTS

In this section, we illustrate the application of the waveform inversion procedure to the laboratory measurement of attenuation using cylindrical bars. The samples used are a PVC material and Sierra White granite. The first is a low velocity and highly attenuative plastic material. The second is a high-Q rock. The elastic properties of the two materials are given in Table 1.

Experimental Procedure

Figure 3 shows a diagram of the measuring system. A pulse generator with various source functions is used to apply an excitation signal to the source transducer. Unlike most pulse transmission measurements where a sharp source pulse is usually used, the present measurement uses a burst-sine wave source with adjustable frequencies. This is because the waveform inversion technique can deal with signals of long duration, while other measurements (e.g., spectral ratio method) require signals of short duration. The signal generator in Figure 3 is adjusted to generate signals with appropriate frequencies within the frequency range of the fundamental wave mode in the cylindrical sample. This requires that the source and receiver transducers have good responses in the (low) frequency range. The measurements are performed on two samples of the same material but different length. The requirement of the same material for the two measurements is based on the consideration that the transmitting and receiving of the source and receiver transducers depend on the elastic properties of the sample, which determine the load impedance of the transducers. Using samples of the same material ensures that measurement conditions such as transducer-sample coupling, signal generation, and signal receiving are the same for both measurements, so that the difference between the two measured waveforms are due to the dispersion and attenuation effects only. In addition, because the waveform inversion technique requires that the two waveforms be aligned in phase before the inversion is applied, the sampling interval of the digital oscilloscope should be fine enough to achieve such an alignment. A sampling rate of about 40-100 points per cycle is recommended.

Results

I first present the results for the PVC bar. The lengths of the short and long samples are 8.28 and 21.82 cm respectively. The radius of the samples is 0.645 cm. Figure 4a shows the measured waveforms for the 8.28 and 21.82 cm samples. The waveforms are measured for the 40 kHz and 60 kHz source signal frequencies. For the shorter sample, the received (40 kHz) signal clearly shows the arrival of the first and second reflections. The time interval between signal onset and the arrival of the first reflection determines ΔT in Eq. (7). For the longer sample, the received waveforms (particularly the 60 kHz signal) exhibit significant distortion due to dispersion and amplitude attenuation due to intrinsic damping. For the given material properties (Table 1) and bar radius, the waveforms at 8.28 cm are theoretically propagated to 21.82 cm to correct for the dispersion effect. The waveform inversion is then applied to derive Q_e from the 40 kHz and 60 kHz waveform pairs. The results of waveform inversion are given in Figure 4b. After the dispersion correction and inversion, the waveforms (both 40 and 60 kHz) at 21.82 cm are satisfactorily recovered from the waveforms at 8.28 cm. Considering the significant distortion of waveforms at 21.82 cm compared with those at 8.28 cm, the results in Figure 4b show that the dispersion correction is effective and sufficiently accurate. Furthermore, the Q_e values obtained from the two different frequencies are very close. They are $Q_e = 14.2$ for 40 kHz and 13.9 for 60 kHz, indicating the consistency of the inversion results.

Of the most interest are the results from the measurements on granite. Resonant bar measurements were performed on the sample before it was cut into two samples of lengths 5.16 and 11.91 cm. The radius of the samples is 0.672 cm. The resonant bar results will be compared with those from the present technique. Figure 5 shows the waveform data from measuring the shorter and longer samples for different source frequencies ranging from 40 to 140 kHz. With increasing frequency, the dispersive features of the waves become more evident. Figure 6 shows the match of the waveforms after the inversion. The matches are generally very good. The inverted Q_e values for these frequencies are given in Figure 6 for each pair of matched waveforms. The Q_e values are on the order of 110. To compare these data with those from the resonant bar measurement, we plot the attenuation data expressed as $1000/Q_e$ versus frequency in Figure 7, together with a value measured on a granite sample using spectral ratio method around 800 kHz. The ultrasonic extensional attenuation value was derived from the measured compressional and shear attenuation values. As seen in this figure, the waveform inversion results (open circles) are quite consistent with the resonant bar results (triangles). The ultrasonic measurement (square) yields significantly higher attenuation than the two low frequency measurements, suggesting that scattering is the mechanism for attenuation at ultrasonic frequencies (Winkler, 1983; Blair, 1990). This may also explain why the waveform inversion results generally show slightly higher attenuation than those of the resonant bar measurement, assuming that at the 100 kHz frequency range there are still some scattering effects.

CONCLUSIONS

This study presents a new approach to attenuation measurements through inversion of waveforms. In fact, the waveform inversion technique is not restricted to bar measurements. It can also be adapted to other pulse transmission measurements. For example, for ultrasonic measurements using samples of large lateral dimensions, the waveform inversion is applicable if the waveforms are corrected for diffraction (or beam spreading) effects of the transducer [illegible]ance. Even for the bar geometry, the technique still has several applications. It can be [illegible] be adapted to measure attenuation under confining pressures appropriate to the *in-situ* [illegible] if the dispersion characteristics of the bar in the presence of a confining medium [illegible] is correctly accounted for. In addition, the waveforms of flexural and tortional [illegible] in a cylindrical bar can also be utilized to estimate the shear attenuation of the bar.

REFERENCES

Blair, D. P., 1982, Measurement of rise times of seismic pulses in rock: *Geophysics*, *47*, 1047–1058.

Blair, D. P., 1990, A direct comparison between vibrational resonance and pulse transmission data for assessment of seismic attenuation in rock: *Geophysics*, *55*, 51–60.

Jones, T. D., 1986, Pore fluids and frequency-dependent wave propagation: *Geophysics*, *51*, 1939–1953.

Kjartansson, E., 1979, Constant-Q wave propagation and attenuation: *J. Geophys. Res.*, *84*, 4737–4738.

Kolsky, H. 1953, *Stress Waves in Solids*, Oxford University Press, London.

Liu, H. P., 1988, Effect of source spectrum on seismic attenuation measurements using the pulse-broadening method: *Geophysics, 53*, 1520–1526.

Moré, J. J., 1978, The Levenberg-Marguard algorithm: Implementation and theory: *Lecture Notes in Mathematics, 53*, edited by G. A. Watson, 105–116.

Ricker, N., 1953, The form and laws of propagation of seismic wavelets: *Geophysics, 20*, 53-67.

Tang, X. M., Toksöz, M. N., and Cheng, C. H., 1990, Elastic wave radiation and diffraction of a piston source: *J. Acoust. Soc. Am, 87*, 1894–1902.

Toksöz, M. N., Johnston, D. H., and Timur, A., 1978, Attenuation of seismic waves in dry and saturated rocks: I. Laboratory measurements: *Geophysics*, *44*, 453–462.

Winkler, K. W., 1983, Frequency dependent ultrasonic properties of high-porosity sandstones: *J. Geophys. Res.*, *88*, 9493–9499.

Medium	ρ (g/cm^3)	V_p (m/sec)	V_s (m/sec)
PVC	1.38	2171	1051
Sierra White Granite	2.67	3593	2456

Table 1: Density ρ, compressional velocity V_p, and shear velocity V_s of the solid used in the measurement.

a.

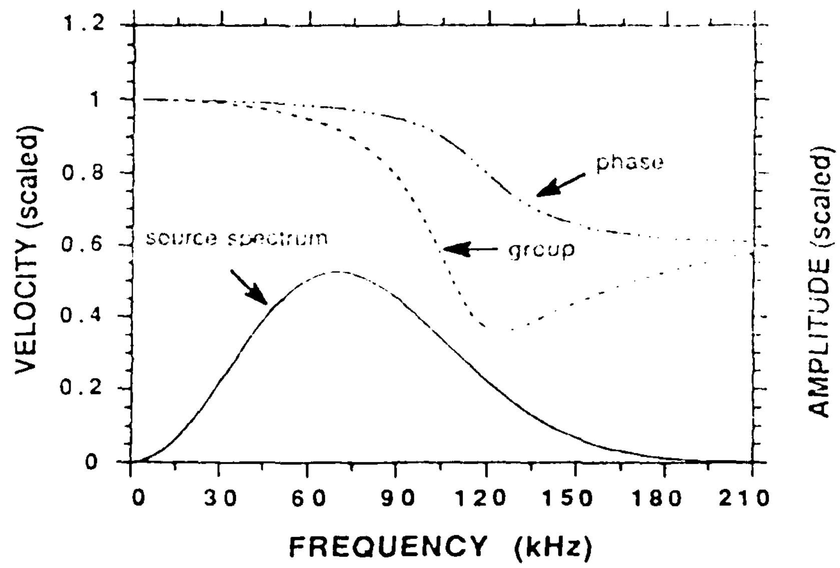

b.

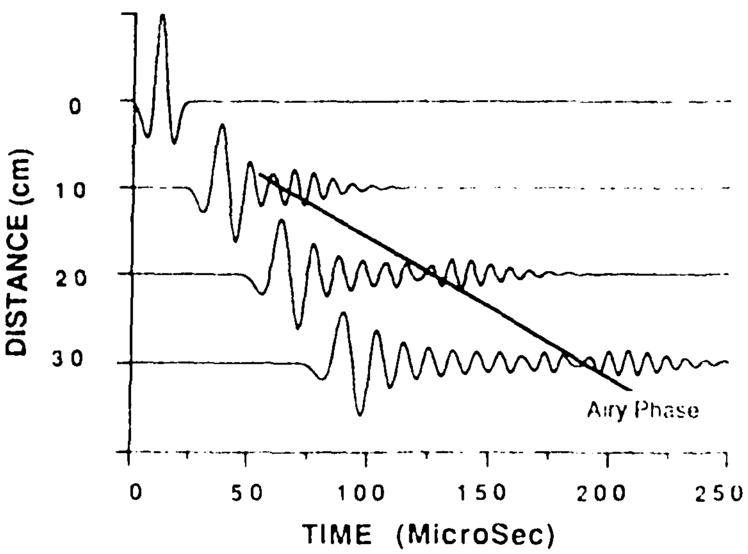

Figure 1: (a) Phase and group velocities (dashed curves) of the cylindrical bar (a = 1 cm, V_p=4272 m/s, and V_s=2506 m/s) in the frequency range covered by the source spectrum (solid curve). The velocities are scaled by V_e = 3943 m/s. (b) Propagation of the fundamental mode in the bar. Note the distortion of waveforms and the development of the Airy phase.

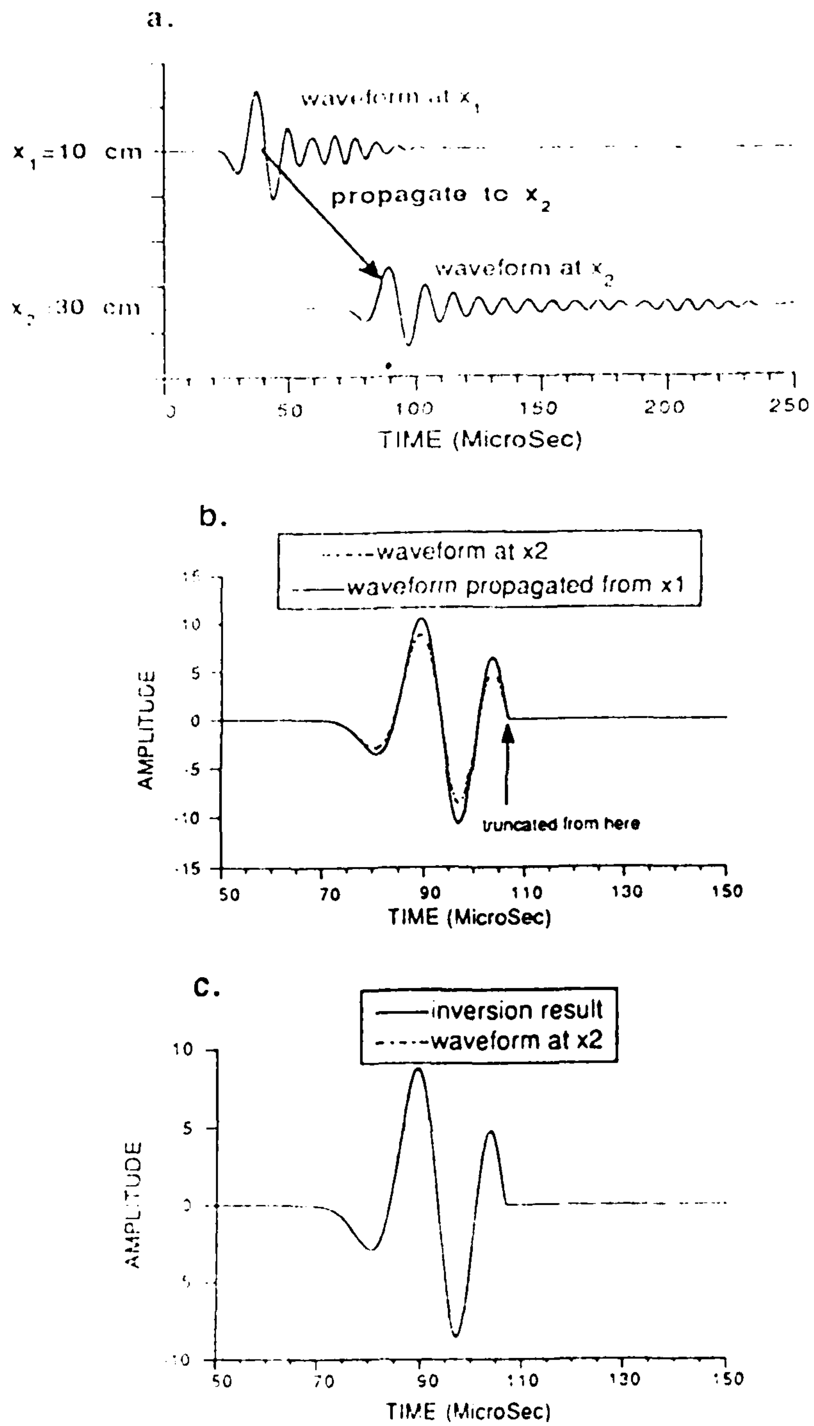

Figure 2: Illustration of the waveform inversion procedure. (a)Propagate waveform at x_1 to x_2. (b)Result of the dispersion correction: the waveforms are aligned in phase; the amplitude difference is due to attenuation and is to be minimized to find Q_e. (c) After inversion, the two waveforms are matched. The Q_e required for the match gives the estimated attenuation.

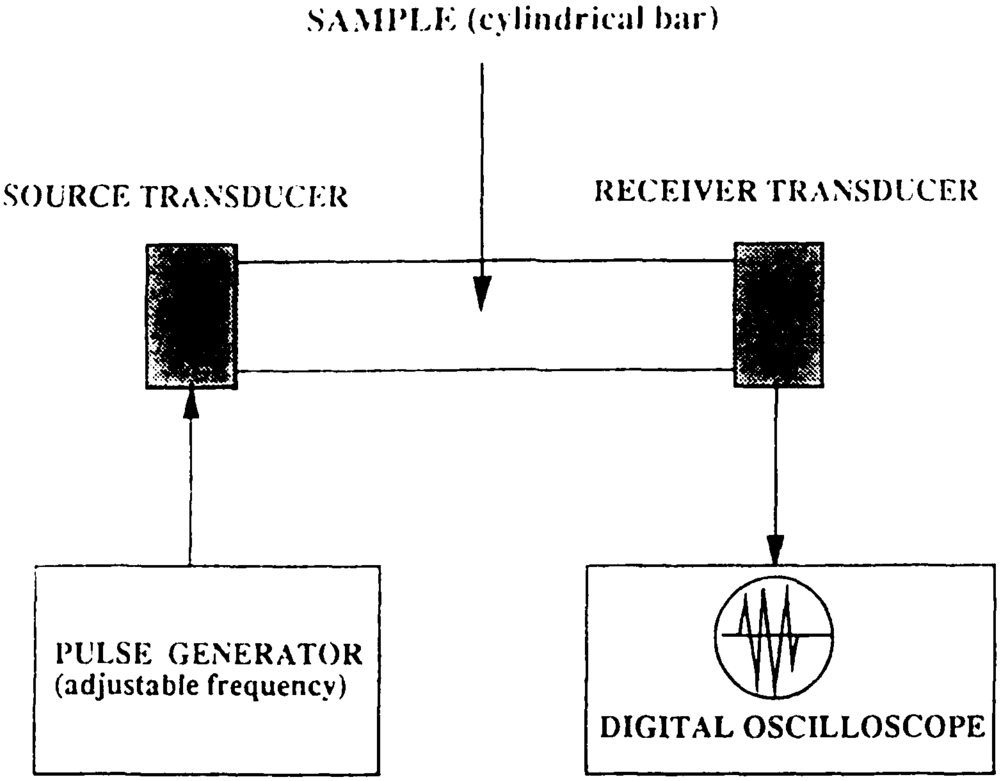

Figure 3: Diagram of the system for measuring attenuation in bars.

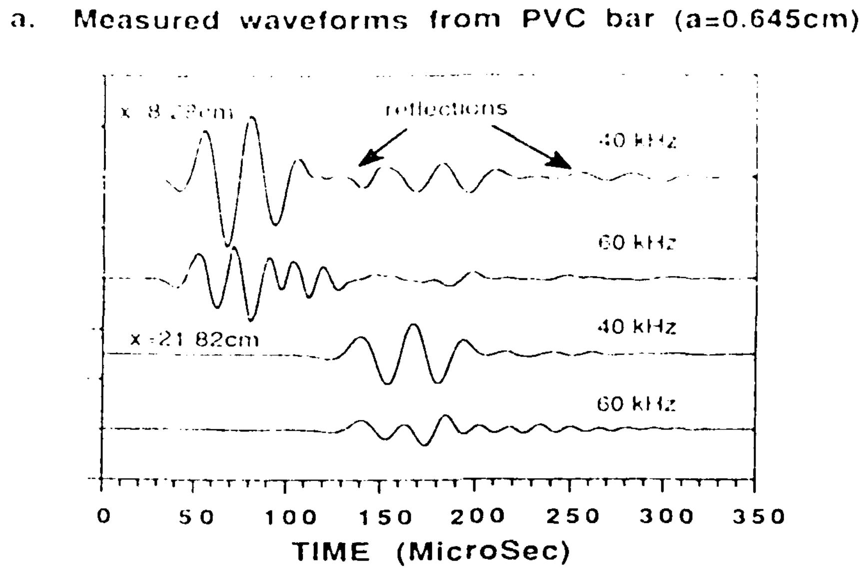

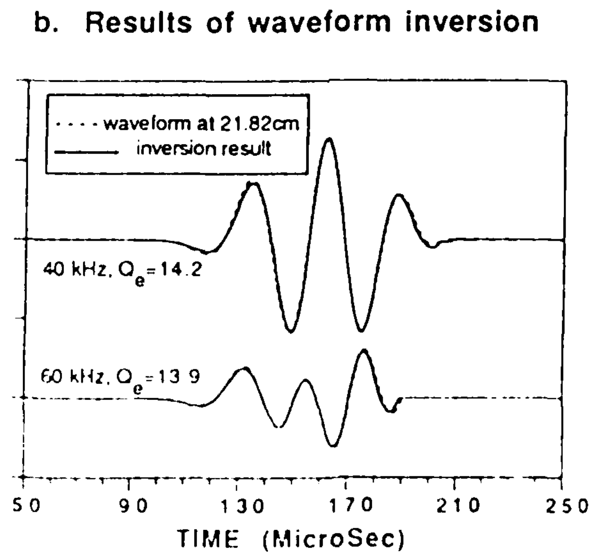

Figure 4: (a) Waveforms measured from the short and long PVC bars at 40 and 60 kHz frequencies. (b)Matched waveforms after the dispersion correction and inversion. The inverted Q_e values for the two frequencies are also indicated.

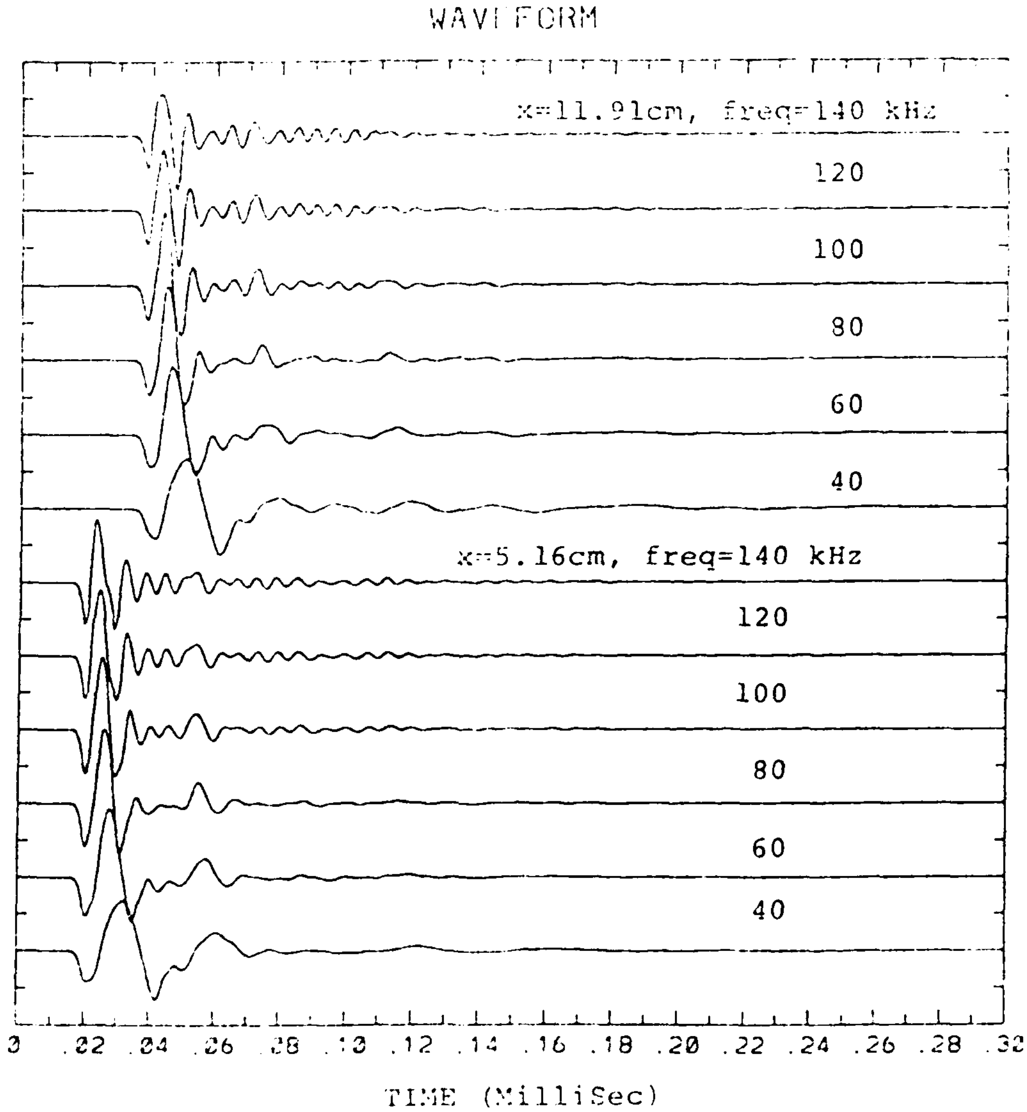

Figure 5: Waveforms measured from the short and long Sierra White granite bars for frequencies ranging from 40 to 140 kHz.

Waveform Inversion Results for Sierra White Granite

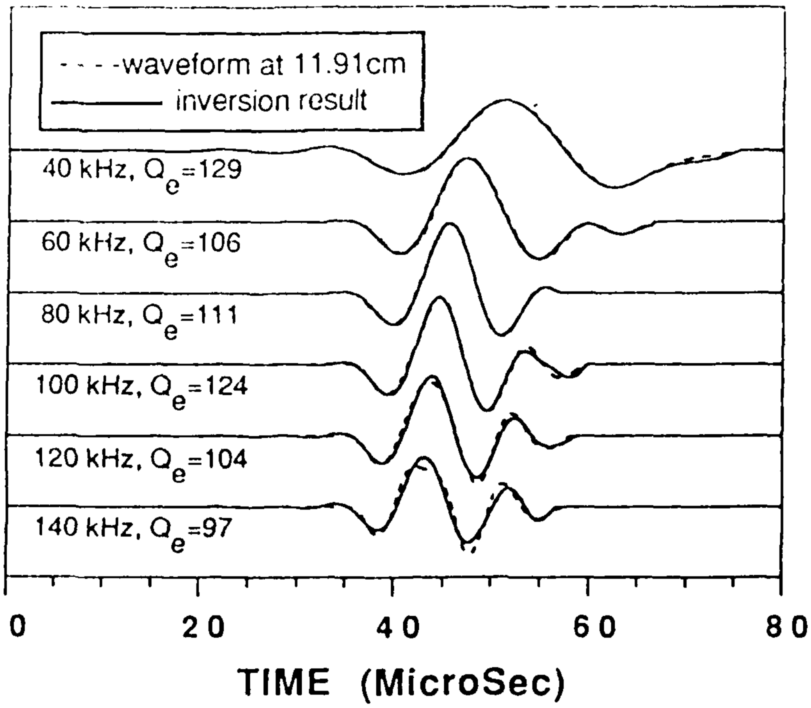

Figure 6: Matched waveforms after the dispersion correction and inversion for the different frequencies. The inverted Q_e values for the frequencies are also indicated.

COMPARISON OF ATTENUATION VALUES OF SIERRA WHITE GRANITE OBTAINED USING DIFFERENT METHODS

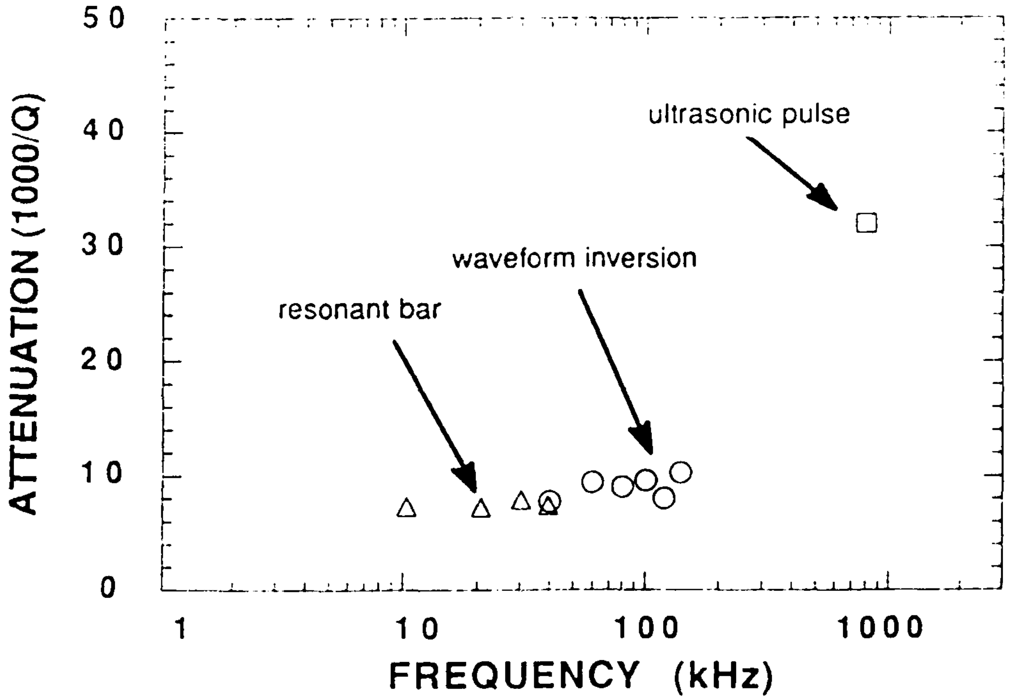

Figure 7: Comparison of extensional attenuations (expressed as 1000/Q) measured using resonant bar (triangles), waveform inversion (open circles), and ultrasonic pulse propagation (square).

CONTRACTORS

Prof. Thomas Ahrens
Seismological Lab, 252-21
Division of Geological & Planetary Sciences
California Institute of Technology
Pasadena, CA 91125

Prof. Keiiti Aki
Center for Earth Sciences
University of Southern California
University Park
Los Angeles, CA 90089-0741

Prof. Shelton Alexander
Geosciences Department
403 Deike Building
The Pennsylvania State University
University Park, PA 16802

Dr. Ralph Alewine, III
DARPA/NMRO
3701 North Fairfax Drive
Arlington, VA 22203-1714

Prof. Charles B. Archambeau
CIRES
University of Colorado
Boulder, CO 80309

Dr. Thomas C. Bache, Jr.
Science Applications Int'l Corp.
10260 Campus Point Drive
San Diego, CA 92121 (2 copies)

Prof. Muawia Barazangi
Institute for the Study of the Continent
Cornell University
Ithaca, NY 14853

Dr. Jeff Barker
Department of Geological Sciences
State University of New York
at Binghamton
Vestal, NY 13901

Dr. Douglas R. Baumgardt
ENSCO, Inc
5400 Port Royal Road
Springfield, VA 22151-2388

Dr. Susan Beck
Department of Geosciences
Building #77
University of Arizona
Tuscon, AZ 85721

Dr. T.J. Bennett
S-CUBED
A Division of Maxwell Laboratories
11800 Sunrise Valley Drive, Suite 1450
Reston, VA 22091

Dr. Robert Blandford
AFTAC/IT, Center for Seismic Studies
1330 North 17th Street
Suite 1450
Arlington, VA 22209-2308

Dr. G.A. Bollinger
Department of Geological Sciences
Virginia Polytechnical Institute
21044 Derring Hall
Blacksburg, VA 24061

Dr. Stephen Bratt
Center for Seismic Studies
1300 North 17th Street
Suite 1450
Arlington, VA 22209-2308

Dr. Lawrence Burdick
Woodward-Clyde Consultants
566 El Dorado Street
Pasadena, CA 91109-3245

Dr. Robert Burridge
Schlumberger-Doll Research Center
Old Quarry Road
Ridgefield, CT 06877

Dr. Jerry Carter
Center for Seismic Studies
1300 North 17th Street
Suite 1450
Arlington, VA 22209-2308

Dr. Eric Chael
Division 9241
Sandia Laboratory
Albuquerque, NM 87185

Prof. Vernon F. Cormier
Department of Geology & Geophysics
U-45, Room 207
University of Connecticut
Storrs, CT 06268

Prof. Anton Dainty
Earth Resources Laboratory
Massachusetts Institute of Technology
42 Carleton Street
Cambridge, MA 02142

Prof. Steven Day
Department of Geological Sciences
San Diego State University
San Diego, CA 92182

Marvin Denny
U.S. Department of Energy
Office of Arms Control
Washington, DC 20585

Dr. Zoltan Der
ENSCO, Inc.
5400 Port Royal Road
Springfield, VA 22151-2388

Prof. Adam Dziewonski
Hoffman Laboratory, Harvard University
Dept. of Earth Atmos. & Planetary Sciences
20 Oxford Street
Cambridge, MA 02138

Prof. John Ebel
Department of Geology & Geophysics
Boston College
Chestnut Hill, MA 02167

Eric Fielding
SNEE Hall
INSTOC
Cornell University
Ithaca, NY 14853

Dr. Mark D. Fisk
Mission Research Corporation
735 State Street
P.O. Drawer 719
Santa Barbara, CA 93102

Prof Stanley Flatte
Applied Sciences Building
University of California, Santa Cruz
Santa Cruz, CA95064

Dr. John Foley
NER-Geo Sciences
1100 Crown Colony Drive
Quincy, MA 02169

Prof. Donald Forsyth
Department of Geological Sciences
Brown University
Providence, RI 02912

Dr. Art Frankel
U.S. Geological Survey
922 National Center
Reston, VA 22092

Dr. Cliff Frolich
Institute of Geophysics
8701 North Mopac
Austin, TX 78759

Dr. Holly Given
IGPP, A-025
Scripps Institute of Oceanography
University of California, San Diego
La Jolla, CA 92093

Dr. Jeffrey W. Given
SAIC
10260 Campus Point Drive
San Diego, CA 92121

Dr. Dale Glover
Defense Intelligence Agency
ATTN: ODT-1B
Washington, DC 20301

Dr. Indra Gupta
Teledyne Geotech
314 Montgomery Street
Alexanderia, VA 22314

Dan N. Hagedon
Pacific Northwest Laboratories
Battelle Boulevard
Richland, WA 99352

Dr. James Hannon
Lawrence Livermore National Laboratory
P.O. Box 808
L-205
Livermore, CA 94550

Dr. Roger Hansen
HHQ AFTAC/TTR
Patrick AFB, FL 32925-6001

Prof. David G. Harkrider
Seismological Laboratory
Division of Geological & Planetary Sciences
California Institute of Technology
Pasadena, CA 91125

Prof. Danny Harvey
CIRES
University of Colorado
Boulder, CO 80309

Prof. Donald V. Helmberger
Seismological Laboratory
Division of Geological & Planetary Sciences
California Institute of Technology
Pasadena, CA 91125

Prof. Eugene Herrin
Institute for the Study of Earth and Man
Geophysical Laboratory
Southern Methodist University
Dallas, TX 75275

Prof. Robert B. Herrmann
Department of Earth & Atmospheric Sciences
St. Louis University
St. Louis, MO 63156

Prof. Lane R. Johnson
Seismographic Station
University of California
Berkeley, CA 94720

Prof. Thomas H. Jordan
Department of Earth, Atmospheric &
Planetary Sciences
Massachusetts Institute of Technology
Cambridge, MA 02139

Prof. Alan Kafka
Department of Geology & Geophysics
Boston College
Chestnut Hill, MA 02167

Robert C. Kemerait
ENSCO, Inc.
445 Pineda Court
Melbourne , FL 32940

Dr. Max Koontz
U.S. Dept. of Energy/DP 5
Forrestal Building
1000 Independence Avenue
Washington, DC 20585

Dr. Richard LaCoss
MIT Lincoln Laboratory, M-200B
P.O. Box 73
Lexington, MA 02173-0073

Dr. Fred K. Lamb
University of Illinois at Urbana-Champaign
Department of Physics
1110 West Green Street
Urbana, IL 61801

Prof. Charles A. Langston
Geosciences Department
403 Deike Building
The Pennsylvania State University
University Park, PA 16802

Jim Lawson, Chief Geophysicist
Oklahoma Geological Survey
Oklahoma Geophysical Observatory
P.O. Box 8
Leonard, OK 74043-0008

Prof. Thorne Lay
Institute of Tectonics
Earth Science Board
University of California, Santa Cruz
Santa Cruz, CA 95064

Dr. William Leith
U.S. Geological Survey
Mail Stop 928
Reston, VA 22092

Mr. James F. Lewkowicz
Phillips Laboratory/GPEH
Hanscom AFB, MA 01731-5000(2 copies)

Mr. Alfred Lieberman
ACDA/VI-OA State Department Building
Room 5726
320-21st Street, NW
Washington, DC 20451

Prof. L. Timothy Long
School of Geophysical Sciences
Georgia Institute of Technology
Atlanta, GA 30332

Dr. Robert Masse
Denver Federal Building
Bos 25046, Mail Stop 967
Denver, CO 80225

Dr. Randolph Martin, III
New England Research, Inc.
76 Olcott Drive
White River Junction, VT 05001

Dr. Gary McCartor
Department of Physics
Southern Methodist University
Dallas, TX 75275

Prof. Thomas V. McEvilly
Seismographic Station
University of California
Berkeley, CA 94720

Dr. Art McGarr
U.S. Geological Survey
Mail Stop 977
U.S. Geological Survey
Menlo Park, CA 94025

Dr. Keith L. McLaughlin
S-CUBED
A Division of Maxwell Laboratory
P.O. Box 1620
La Jolla, CA 92038-1620

Stephen Miller & Dr. Alexander Florence
SRI International
333 Ravenswood Avenue
Box AF 116
Menlo Park, CA 94025-3493

Prof. Bernard Minster
IGPP, A-025
Scripps Institute of Oceanography
University of California, San Diego
La Jolla, CA 92093

Prof. Brian J. Mitchell
Department of Earth & Atmospheric Sciences
St. Louis University
St. Louis, MO 63156

Mr. Jack Murphy
S-CUBED
A Division of Maxwell Laboratory
11800 Sunrise Valley Drive, Suite 1212
Reston, VA 22091 (2 Copies)

Dr. Keith K. Nakanishi
Lawrence Livermore National Laboratory
L-025
P.O. Box 808
Livermore, CA 94550

Dr. Carl Newton
Los Alamos National Laboratory
P.O. Box 1663
Mail Stop C335, Group ESS-3
Los Alamos, NM 87545

Dr. Bao Nguyen
HQ AFTAC/TTR
Patrick AFB, FL 32925-6001

Prof. John A. Orcutt
IGPP, A-025
Scripps Institute of Oceanography
University of California, San Diego
La Jolla, CA 92093

Prof. Jeffrey Park
Kline Geology Laboratory
P.O. Box 6666
New Haven, CT 06511-8130

Dr. Howard Patton
Lawrence Livermore National Laboratory
L-025
P.O. Box 808
Livermore, CA 94550

Dr. Frank Pilotte
HQ AFTAC/TT
Patrick AFB, FL 32925-6001

Dr. Jay J. Pulli
Radix Systems, Inc.
2 Taft Court, Suite 203
Rockville, MD 20850

Dr. Robert Reinke
ATTN: FCTVTD
Field Command
Defense Nuclear Agency
Kirtland AFB, NM 87115

Prof. Paul G. Richards
Lamont-Doherty Geological Observatory
of Columbia University
Palisades, NY 10964

Mr. Wilmer Rivers
Teledyne Geotech
314 Montgomery Street
Alexandria, VA 22314

Dr. George Rothe
HQ AFTAC/TTR
Patrick AFB, FL 32925-6001

Dr. Alan S. Ryall, Jr.
DARPA/NMRO
3701 North Fairfax Drive
Arlington, VA 22209-1714

Prof. David G. Simpson
IRIS, Inc.
1616 North Fort Myer Drive
Suite 1400
Arlington, VA 22209

Dr. Richard Sailor
TASC, Inc.
55 Walkers Brook Drive
Reading, MA 01867

Donald L. Springer
Lawrence Livermore National Laboratory
L-025
P.O. Box 808
Livermore, CA 94550

Prof. Charles G. Sammis
Center for Earth Sciences
University of Southern California
University Park
Los Angeles, CA 90089-0741

Dr. Jeffrey Stevens
S-CUBED
A Division of Maxwell Laboratory
P.O. Box 1620
La Jolla, CA 92038-1620

Prof. Christopher H. Scholz
Lamont-Doherty Geological Observatory
of Columbia University
Palisades, CA 10964

Lt. Col. Jim Stobie
ATTN: AFOSR/NL
Bolling AFB
Washington, DC 20332-6448

Dr. Susan Schwartz
Institute of Tectonics
1156 High Street
Santa Cruz, CA 95064

Prof. Brian Stump
Institute for the Study of Earth & Man
Geophysical Laboratory
Southern Methodist University
Dallas, TX 75275

Secretary of the Air Force
(SAFRD)
Washington, DC 20330

Prof. Jeremiah Sullivan
University of Illinois at Urbana-Champaign
Department of Physics
1110 West Green Street
Urbana, IL 61801

Office of the Secretary of Defense
DDR&E
Washington, DC 20330

Prof. L. Sykes
Lamont-Doherty Geological Observatory
of Columbia University
Palisades, NY 10964

Thomas J. Sereno, Jr.
Science Application Int'l Corp.
10260 Campus Point Drive
San Diego, CA 92121

Dr. David Taylor
ENSCO, Inc.
445 Pineda Court
Melbourne, FL 32940

Dr. Michael Shore
Defense Nuclear Agency/SPSS
6801 Telegraph Road
Alexandria, VA 22310

Dr. Steven R. Taylor
Los Alamos National Laboratory
P.O. Box 1663
Mail Stop C335
Los Alamos, NM 87545

Dr. Matthew Sibol
Virginia Tech
Seismological Observatory
4044 Derring Hall
Blacksburg, VA 24061-0420

Prof. Clifford Thurber
University of Wisconsin-Madison
Department of Geology & Geophysics
1215 West Dayton Street
Madison, WS 53706

Prof. M. Nafi Toksoz
Earth Resources Lab
Massachusetts Institute of Technology
42 Carleton Street
Cambridge, MA 02142

Dr. Larry Turnbull
CIA-OSWR/NED
Washington, DC 20505

Dr. Gregory van der Vink
IRIS, Inc.
1616 North Fort Myer Drive
Suite 1440
Arlington, VA 22209

Dr. Karl Veith
EG&G
5211 Auth Road
Suite 240
Suitland, MD 20746

Prof. Terry C. Wallace
Department of Geosciences
Building #77
University of Arizona
Tuscon, AZ 85721

Dr. Thomas Weaver
Los Alamos National Laboratory
P.O. Box 1663
Mail Stop C335
Los Alamos, NM 87545

Dr. William Wortman
Mission Research Corporation
8560 Cinderbed Road
Suite 700
Newington, VA 22122

Prof. Francis T. Wu
Department of Geological Sciences
State University of New Yor
at Binghamton
Vestal, NY 13901

AFTAC/CA
(STINFO)
Patrick AFB, FL 32925-6001

DARPA/PM
3701 North Fairfax Drive
Arlington, VA 22203-1714

DARPA/RMO/RETRIEVAL
3701 North Fairfax Drive
Arlington, VA 22203-1714

DARPA/RMO/SECURITY OFFICE
3701 North Fairfax Drive
Arlington, VA 2203-1714

HQ DNA
ATTN: Technical Library
Washington, DC 20305

Defense Intelligence Agency
Directorate for Scientific & Technical Intelligence
ATTN: DTIB
Washington, DC 20340-6158

Defense Technical Information Center
Cameron Station
Alexandria, VA 22314 (2 Copies)

TACTEC
Battelle Memorial Institute
505 King Avenue
Columbus, OH 43201 (Final Report)

Phillips Laboratory
ATTN: XPG
Hanscom AFB, MA 01731-5000

Phillips Laboratory
ATTN: GPE
Hanscom AFB, MA 01731-5000

Phillips Laboratory
ATTN: TSML
Hanscom AFB, MA 01731-5000

Phillips Laboratory
ATTN: SUL
Kirtland, NM 87117 (2 copies)

Dr. Michel Bouchon
I.R.I.G.M.-B.P. 68
38402 St. Martin D'Heres
Cedex, FRANCE

Dr. Michel Campillo
Observatoire de Grenoble
I.R.I.G.M.-B.P. 53
38041 Grenoble, FRANCE

Dr. Kin Yip Chun
Geophysics Division
Physics Department
University of Toronto
Ontario, CANADA

Prof. Hans-Peter Harjes
Institute for Geophysic
Ruhr University/Bochum
P.O. Box 102148
4630 Bochum 1, GERMANY

Prof. Eystein Husebye
NTNF/NORSAR
P.O. Box 51
N-2007 Kjeller, NORWAY

David Jepsen
Acting Head, Nuclear Monitoring Section
Bureau of Mineral Resources
Geology and Geophysics
G.P.O. Box 378, Canberra, AUSTRALIA

Ms. Eva Johannisson
Senior Research Officer
National Defense Research Inst.
P.O. Box 27322
S-102 54 Stockholm, SWEDEN

Dr. Peter Marshall
Procurement Executive
Ministry of Defense
Blacknest, Brimpton
Reading FG7-FRS, UNITED KINGDOM

Dr. Bernard Massinon, Dr. Pierre Mechler
Societe Radiomana
27 rue Claude Bernard
75005 Paris, FRANCE (2 Copies)

Dr. Svein Mykkeltveit
NTNT/NORSAR
P.O. Box 51
N-2007 Kjeller, NORWAY (3 Copies)

Prof. Keith Priestley
University of Cambridge
Ballard Labs, Dept. of Earth Sciences
Madingley Rise, Madingley Road
Cambridge CB3 OEZ, ENGLAND

Dr. Jorg Schlittenhardt
Federal Institute for Geosciences & Nat'l Res.
Postfach 510153
D-3000 Hannover 51, GERMANY

Dr. Johannes Schweitzer
Institute of Geophysics
Ruhr University/Bochum
P.O. Box 1102148
4360 Bochum 1, GERMANY